Optical Engineering

SPIEDigitalLibrary.org/oe

Parametric analysis of the effect of scattered light upon the modulation transfer function

James E. Harvey

Parametric analysis of the effect of scattered light upon the modulation transfer function

James E. Harvey
Photon Engineering
LLC, 440 S. Williams Boulevard
Suite 106 Tucson, Arizona 85711
E-mail: jimh@photonengr.com

Abstract. The modulation transfer function (MTF) is widely used as the image quality criterion of choice for imaging applications where fine detail in extended images needs to be specified or evaluated. We present a parametric analysis of the effect of scattered light upon the MTF of an imaging system and illustrate the results for three specific applications: (1) a visible Newtonian telescope with moderately good optical surfaces which produce no significant effect upon the MTF, (2) an extreme ultraviolet Newtonian telescope where scattering effects can dominate both diffraction effects and aberrations in the resulting image degradation even for state-of-the-art optical surfaces, and (3) a visible system made up of three diamond-turned off-axis aspheric mirrors where we use the predicted MTF to estimate whether post-polishing is required (huge cost and schedule impact) to meet a specific image quality requirement. [DOI: 10.1117/1.OE.52.7.073110]

Subject terms: modulation transfer function due to surface scatter; modulation transfer function; image degradation.

Paper 130568 received Apr. 15, 2013; revised manuscript received Jun. 24, 2013; accepted for publication Jun. 25, 2013; published online Jul. 29, 2013.

1 Introduction

The modulation transfer function (MTF) is widely used as the image quality criterion of choice for imaging applications where fine detail in extended images needs to be specified or evaluated.[1–3] This is particularly true for imaging systems degraded by diffraction effects and geometrical aberrations. However, there seems to be a dearth of optical engineering literature concerning the effects of scattered light upon the MTF. Exceptions include the medical x-ray imaging community involved in projection mammography[4] and the vision community where intraocular scattering effects are of concern.[5]

In this article, we present a detailed parametric analysis of the effect of scattered light from residual optical fabrication errors upon the MTF of an imaging system. After a brief historical background of surface scatter theory, we review the evolution of a linear systems formulation of surface scatter theory that characterizes the surface scatter behavior by a surface transfer function (STF). This STF can merely be multiplied by the classical optical transfer function (OTF) characterizing image degradation by diffraction effects and geometrical aberrations to obtain the composite MTF for systems also degraded by surface scatter effects. Insight into the magnitude of image degradation due to surface scatter is then provided by performing a detailed parametric analysis of MTF behavior for surfaces with a Gaussian surface power spectral density (PSD) function. The parameters varied include the surface-roughness-to-wavelength ratio, surface correlation width, and incident angle. The resulting parametric plots provide the optical engineer with insight and understanding concerning the relative importance of diffraction and scattering that is not readily available in the currently existing literature.

This analysis is first applied to a Newtonian telescope with moderately good mirrors operating at visible wavelengths. The resulting image degradation due to scattered light is barely perceptible. We then apply the analysis to the same Newtonian telescope with state-of-the-art mirror surfaces operating at extreme ultraviolet (EUV) wavelengths ranging from 300 to 100 Å. At the long wavelength end of this spectral range diffraction effects dominate the scatter effects; however, at the shortest wavelengths, surface scatter effects dominate the diffraction. A third application involves a system made up of three diamond-turned off-axis aspheric mirrors operating at a wavelength of 600 nm in the visible. We demonstrate how the predicted MTF can be used to estimate whether post-polishing will be required to meet a specific image quality requirement.

Finally, we briefly discuss how to use commercially available state-of-the-art optical analysis software to calculate the MTF degradation due to stray light from bulk or particulate scatter provided either measured or assumed bidirectional reflectance distribution function (BRDF) data is available.

2 Historical Background of Surface Scatter Theory

Scattering effects from microtopographic surface roughness are merely nonparaxial diffraction phenomena resulting from random phase variations in the reflected wavefront. Rayleigh–Rice[6–8] or Beckmann–Kirchhoff[9] theories are commonly used to predict surface scatter effects. Also, Harvey and Shack (1976) developed a linear systems formulation of surface scatter phenomena in which the scattering behavior is characterized by a STF.[10,11] This treatment provided insight and understanding not readily gleaned from the two previous theories. However, smooth surface and/or paraxial approximations have severely limited the range of applicability in each of the above theoretical treatments.

The Rayleigh–Rice vector perturbation theory agrees well with experimental wide-angle scatter measurements from "smooth" ($4\pi\sigma_{\mathrm{rel}} \cos\theta_i/\lambda \ll 1$) surfaces for arbitrary

incident and scattering angles. However, not all applications of interest satisfy the smooth surface approximation. The Beckmann–Kirchhoff scattering theory is valid for rougher surfaces; but it contains a paraxial (small angle) assumption that limits its ability to accurately handle wide-angle scattering and large angles of incidence. The two most widely used surface scattering theories are thus complementary but not all-inclusive; i.e., neither of them, nor the combination of them, adequately describes scattering behavior for moderately rough surfaces with a large incident and scattering angles.

The original Harvey–Shack (OHS) surface scatter theory has, essentially, the same limitations as the Beckmann–Kirchhoff theory. This transfer function characterization of scattering surfaces was modified in the 1980s to include grazing-incidence effects in x-ray telescopes; however, it was still limited to small-angle scattering.[12]

In 2004, Elfouhaily and Guerin conducted a critical survey of approximate scattering wave theories from random rough surfaces.[13] They attempted to classify and characterize >30 different approximate methods. These were all variants of the small perturbation method (Rayleigh–Rice), the Kirchhoff approach, or so-called unified methods which tried to bridge the gap between the two. This exhaustive survey included 260 references. They concluded that "there does not seem to be a universal method that is to be preferred systematically. All methods present a compromise between versatility, simplicity, numerical efficiency, accuracy and robustness." Their final statement was, "There is still room for improvement in the development of approximate scattering methods."

In 1998, an empirical modification of the Beckmann–Kirchhoff surface scatter theory was developed that appeared to satisfactorily combine the advantages of both the Rayleigh–Rice and the Beckmann–Kirchhoff theories without the disadvantages of either.[14] However, because it was empirically developed rather than theoretically derived, this work was not published in the archival literature until 2007.[15] During this time interval, the modified Beckmann–Kirchhoff surface scatter model was evaluated, implemented, and referenced by researchers in the computer vision and computer animation fields who are less interested in rigorously solving the surface scatter problem than merely having a surface scatter model that results in the rendering of realistic surfaces, textures, objects, and scenes under a wide variety of illumination conditions.[16–24]

A new linear systems formulation of nonparaxial scalar diffraction theory[25,26] applied to surface scatter phenomena eventually resulted in a generalized Harvey–Shack (GHS) surface scatter theory that produces accurate results for rougher surfaces than the Rayleigh–Rice theory and for larger incident and scattered angles than the classical Beckmann–Kirchhoff theory.[27,28]

3 Transfer Function Characterization of Scattering Surfaces

The well-known linear systems formulation of image formation is illustrated schematically in Fig. 1. The irradiance distribution in the image of a point source, or point spread function (PSF), of the imaging system is given by the squared modulus of the Fourier transform of the complex pupil function. From the autocorrelation theorem of Fourier

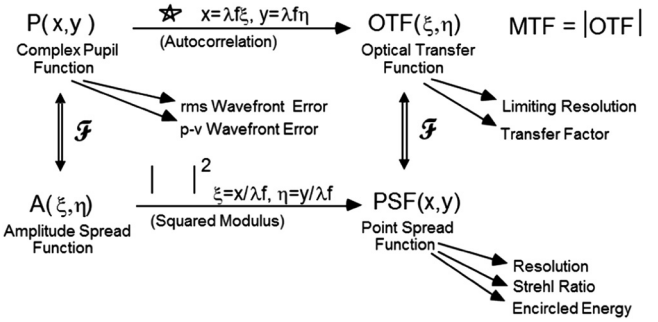

Fig. 1 Schematic diagram of the linear systems formulation of image formation theory.

transform theory, the PSF is also given by the Fourier transform of the autocorrelation of the complex pupil function. The OTF is defined as the (normalized) autocorrelation of the complex pupil function. The OTF and the PSF thus constitute a Fourier transform pair. A variety of commonly used image quality criteria are also added to the diagram, indicating from which function they are most readily obtained.

The imaging system must be isoplanatic (or shift invariant) if a given OTF is going to completely characterize the system. If any field-dependent aberrations are present, a separate OTF is required for each field angle.

Figure 2 schematically illustrates the statistical surface characteristics in a very reminiscent manner of the diagram in Fig. 1. Note that the surface autocovariance (ACV) function and the surface PSD function constitute a Fourier transform pair.

One can now formulate a linear systems theory of surface scatter phenomena by deriving an analytic expression for a STF in much the same way that the OTF was derived in image formation theory.[10,27,28]

3.1 *OHS Surface Scatter Theory*

In the OHS surface scatter theory, paraxial assumptions were made that resulted in the following simple expression for the STF.[10,11]

$$H_s(\hat{x},\hat{y}) = \exp\{-(4\pi\hat{\sigma}_s)^2[1 - C_s(\hat{x},\hat{y})/\sigma_s^2]\}, \quad (1)$$

where σ_s is the rms surface roughness and $C_s(\hat{x},\hat{y})$ is the surface ACV function. The scattered light distribution, called an angle spread function (ASF) in analogy with the PSF of

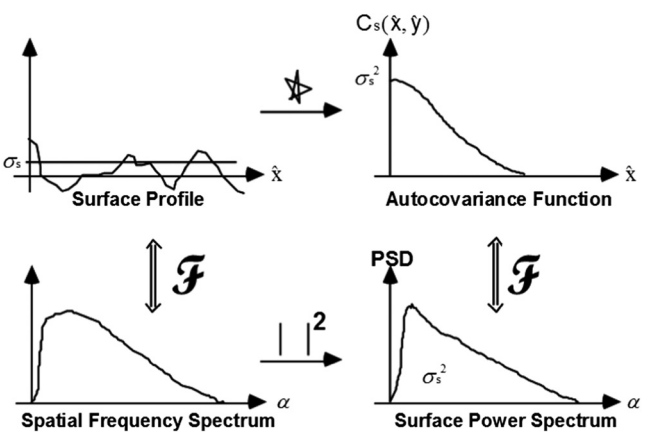

Fig. 2 Schematic diagram of the statistical surface characteristics.

imaging systems, is given by the Fourier transform of this STF.

The STF can also be written in the form

$$H(\hat{x},\hat{y}) = A + BG(\hat{x},\hat{y}) \tag{2}$$

where

$$A = \exp[-(4\pi\hat{\sigma}_s)^2], \tag{3}$$

and

$$B = 1 - \exp[-(4\pi\hat{\sigma}_s)^2] \tag{4}$$

are the fraction of the total reflected radiant power contained in the specular and the scattered components, respectively, and

$$G(\hat{x},\hat{y}) = \frac{\exp[(4\pi)^2 C_s(\hat{x},\hat{y})] - 1}{\exp(4\pi\hat{\sigma}_s)^2 - 1}. \tag{5}$$

From Eq. (2), we see that the STF can be written as the sum of two separate components. The ASF can therefore be expressed as the sum of the Fourier transforms of the two components making up the STF:

$$\mathrm{ASF}(\alpha,\beta) = \mathcal{F}\{H(\hat{x},\hat{y})\} = A\delta(\alpha,\beta) + S(\alpha,\beta), \tag{6}$$

where the scattering function, $S(\alpha,\beta)$, is given by

$$S(\alpha,\beta) = B\mathcal{F}[G(\hat{x},\hat{y})]. \tag{7}$$

Note that a scaled coordinate system has been used in which the spatial variables are normalized by the wavelength of the light ($\hat{x} = x/\lambda$, $\hat{y} = y/\lambda$, etc.). The reciprocal variables α and β are thus the direction cosines of the propagation vectors of the angular spectrum of plane waves discussed by Goodman,[29] Gaskill,[30] and Ratcliff.[31] These direction cosines α, β, and γ are related to the angular variables θ and ϕ in conventional spherical coordinates by the following expressions[32]:

$$\alpha = \sin\theta\cos\phi, \quad \beta = \sin\theta\sin\phi, \quad \gamma = \cos\theta. \tag{8}$$

It is only in this direction cosine space that diffraction (and surface scatter) phenomena exhibit shift-invariant behavior with changes in incident angle, and the radiometric quantity that exhibits this behavior is the diffracted (or scattered) radiance, not intensity or irradiance.[25,33]

Figure 3 graphically illustrates the form of this STF and its associated ASF. The STF is made up of a constant A plus a bell-shaped component of height B. These two components transform into a delta function and a scattering function, respectively. The scattering surface therefore reflects an incident beam of light as a specularly reflected beam (the delta function) of diminished intensity surrounded by a halo of scattered light. From the central ordinate theorem of Fourier transform theory, the volume under the scattering function is equal to B, but $A + B = 1$, hence B is equal to a quantity widely referred to as the total integrated scatter (TIS).[34]

The ASF and the corresponding scattering function are scattered radiance functions, which are consistent with the fact that the BRDF was defined by Nicodemus in 1970 as

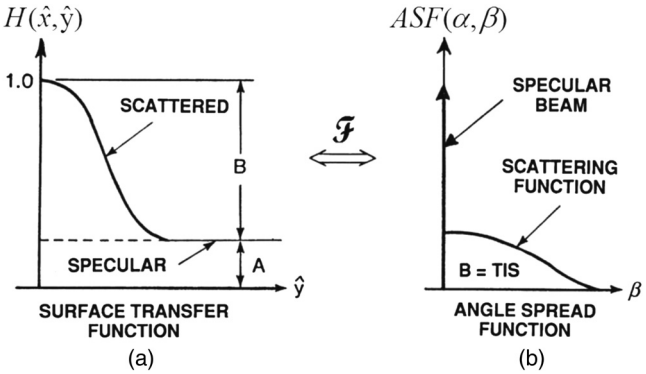

Fig. 3 Illustration of the surface transfer function (STF) and the angle spread function of a scattering surface.

the reflected (or scattered) radiance divided by the incident irradiance:[35]

$$\mathrm{BRDF} = f(\theta_s,\varphi_s,\theta_i,\varphi_i) = \frac{\mathrm{d}L(\theta_s,\varphi_s,\theta_i,\varphi_i)}{\mathrm{d}E(\theta_i,\varphi_i)}. \tag{9}$$

Although there was no explicit smooth surface approximation in this OHS surface scatter theory, the derivation of Eq. (1) did suffer from the same paraxial limitations as the classical Beckmann–Kirchhoff theory. However, for a broad class of scattering surfaces, including optical surfaces polished with conventional techniques on ordinary glassy amorphous materials, the ASF exhibits near shift-invariant behavior in direction cosine space with respect to the incident angle.[11] This led to a modest following among the radiometric community of BRDF curves plotted in the Harvey-Shack $\beta - \beta_o$ format. Breault made an extensive use of this format in building a catalog of BRDF data from various materials and surfaces for use in his APART baffle design program.[36] Today the ASAP, FRED, Trace-Pro, and ZEMAX codes all use some form of the Harvey-Shack BRDF model.[37–40]

Also, if one does make the smooth surface approximation, the quantity $G(\hat{x},\hat{y})$ reduces to the normalized surface ACV function, $C_s(\hat{x},\hat{y})/\sigma_s^2$, and the scattering function becomes proportional to the surface PSD function as predicted by the classical Rayleigh–Rice theory.[6–8]

3.2 *Modified Harvey-Shack Surface Scatter Theory*

The above transfer function characterization of scattering surfaces was modified in the 1980s to include grazing incidence effects in X-ray telescopes, and "mid" spatial frequency surface errors that span the gap between "figure" and "finish" errors.[12] This allowed an understanding of image degradation due to scattering effects from residual optical fabrication errors on NASA's Chandra Observatory and NOAA's Solar X-ray Imager.[41,42]

Krywonos has shown that the STF for an arbitrary incident angle (assuming small angle scattering) can be expressed as[27,28]

$$H_s(\hat{x},\hat{y};\gamma_i) = \exp\{-(4\pi\gamma_i\hat{\sigma}_{\mathrm{rel}})^2[1 - C_s(\hat{x},\hat{y})/\sigma_s^2]\}. \tag{10}$$

This can again be written in the form

$$H_s(\hat{x},\hat{y};\gamma_i) = A(\gamma_i) + B(\gamma_i)G(\hat{x},\hat{y};\gamma_i), \tag{11}$$

where

$$A(\gamma_i) = \exp[-(4\pi\gamma_i\hat{\sigma}_{\mathrm{rel}})^2],\ B(\gamma_i) = 1 - \exp[-(4\pi\gamma_i\hat{\sigma}_{\mathrm{rel}})^2], \tag{12}$$

and

$$G(\hat{x},\hat{y};\gamma_i) = \frac{\exp[(4\pi\gamma_i)^2 C_s(\hat{x},\hat{y})] - 1}{\exp[(4\pi\gamma_i\hat{\sigma}_{\mathrm{rel}})^2] - 1}. \tag{13}$$

In Eq. (10), we have used the relevant surface roughness, σ_{rel}, since spatial frequencies lying outside of the band-limited portion of the surface PSD do not contribute to the scattered radiation.[28] The surface ACV function is divided by the total, or intrinsic, rms roughness, σ_s, as its purpose is to normalize the height of the surface ACV function to unity.

A wavefront incident on the scattering surface at an angle θ_i is equivalent to introducing a linear phase variation across the pupil. Assuming the plane of incidence to be the y-z plane, this will cause a shift of the scattering function in direction cosine space of $\beta - \beta_o$, where $\beta = \sin\theta$ and $\beta_o = \sin\theta_o$. The ASF is therefore given by the Fourier transform of the STF in Eq. (10), or Eq. (11), multiplied by the linear phase variation:

$$\begin{aligned}\mathrm{ASF}(\alpha,\beta-\beta_o;\gamma_i) &= \mathcal{F}\{H_s(\hat{x},\hat{y};\gamma_i)\exp(-i2\pi\hat{y}\beta_o)\}\\ &= A(\gamma_i)\delta(\alpha,\beta-\beta_o) + S(\alpha,\beta-\beta_o;\gamma_i),\end{aligned} \tag{14}$$

where

$$S(\alpha,\beta-\beta_o;\gamma_i) = B(\gamma_i)\mathcal{F}\{G(\hat{x},\hat{y};\gamma_i)\exp(-i2\pi\hat{y}\beta_{\mathrm{o}})\} \quad \text{and} \quad \beta_o - \beta_i. \tag{15}$$

This is again the sum of a delta function at the location of the specular direction surrounded by a scattering function, S, where the fraction of the total reflected power in the specular beam is given by $A(\gamma_i)$, and the fraction of total reflected power in the scattering function (TIS) is given by $B(\gamma_i)$. Hence, $A(\gamma_i) + B(\gamma_i) = 1$, and the ASF again has unit volume.

If any portion of the scattering function S in Eq. (15) falls outside of the unit circle in direction cosine space, it will need to be truncated and renormalized as dictated by Parseval's theorem (also assures conservation of energy). This is accomplished in the same manner as was done for diffraction in Sec. 2 of Ref. 25. The renormalization constant, K, for the scattering function is given by

$$K(\gamma_i) = B(\gamma_i)\left(\int_{\alpha=-1}^{1}\int_{\beta=-\sqrt{1-\alpha^2}}^{\sqrt{1-\alpha^2}} S(\alpha,\beta-\beta_o;\gamma_i)\mathrm{d}\alpha\mathrm{d}\beta\right)^{-1}, \tag{16}$$

and only differs from unity for large incident and scattered angles where the scattering radiance distribution function extends beyond the unit circle in direction cosine space (i.e., only if evanescent waves are produced).[25] The renormalized ASF is thus given by

$$\mathrm{ASF}'(\alpha,\beta-\beta_o;\gamma_i) = K(\gamma_i)\mathcal{F}\{H_s(\hat{x},\hat{y};\gamma_i)\exp(-i2\pi\beta_o\hat{y})\}. \tag{17}$$

Recall that the ASF is a radiance function of unit volume. We can convert the ASF to radiant intensity by multiplying it by the total reflected radiant power and the Lambert's cosine function

$$I(\alpha,\beta-\beta_o;\gamma_i) = \mathrm{RP}_i\mathrm{ASF}'(\alpha,\beta-\beta_o;\gamma_i)\cos\theta_s. \tag{18}$$

Clearly, the surface scatter process is no longer strictly shift invariant with respect to incident angle as reported in Refs. 10 and 11 since Eq. (10) can be interpreted as a one-parameter family of STFs; i.e., a different STF is required for each incident angle. This is analogous to imaging in the presence of field-dependent aberrations, where a different OTF is required for each field angle.

3.3 *GHS Surface Scatter Theory*

The modified version of the Harvey–Shack theory was shown to be a significant improvement over the OHS theory in Ref. 28, especially for large incident angles. However, the restriction of small scattering angles is still very limiting. Furthermore, the OHS and MHS scattering theories were restricted to mirror surfaces and did not include the more general situation of scattering from a random rough surface between two media with arbitrary refractive indices.[43]

Again Krywonos has shown that the following two-parameter family of STFs is required to characterize the scattering process for arbitrary incident and scattering angles:[28]

$$\begin{aligned}H_s(\hat{x},\hat{y};\gamma_i,\gamma_s) &= \exp\{-[2\pi\hat{\sigma}_{\mathrm{rel}}(n_1\gamma_i \mp n_2\gamma_s)]^2\\ &\quad\times[1 - C_s(\hat{x},\hat{y})/\sigma_s^2]\}.\end{aligned} \tag{19}$$

This general expression for the STF may be used to model either reflective or transmissive surface scatter; however, the discussion in this article will be restricted to applications of scattering from mirror surfaces, i.e., $n_2 = -n_1$. If the mirror is immersed in air (or vacuum), $n_1 = 1$ and Eq. (19) can be written as

$$\begin{aligned}H_s(\hat{x},\hat{y};\gamma_i,\gamma_s) &= \exp\{-[2\pi\sigma_{\mathrm{rel}}(\gamma_i + \gamma_s)]^2\\ &\quad\times[1 - C_s(\hat{x},\hat{y})/\sigma_s^2]\}.\end{aligned} \tag{20}$$

Once again, the STF can be written in the form

$$H_s(\hat{x},\hat{y};\gamma_i,\gamma_s) = A(\gamma_i,\gamma_s) + B(\gamma_i,\gamma_s)G(\hat{x},\hat{y};\gamma_i,\gamma_s), \tag{21}$$

$$A(\gamma_i,\gamma_s) = \exp\{-[2\pi(\gamma_i + \gamma_s)\hat{\sigma}_{\mathrm{rel}}]^2\}, \tag{22}$$

where

$$B(\gamma_i,\gamma_s) = 1 - \exp\{-[2\pi(\gamma_i + \gamma_s)\hat{\sigma}_{\mathrm{rel}}]^2\}, \tag{23}$$

$$G(\hat{x},\hat{y};\gamma_i,\gamma_s) = \frac{\exp\left\{[2\pi(\gamma_i+\gamma_s)]^2\frac{\sigma_{\mathrm{rel}}^2}{\sigma_s^2}C_s(\hat{x},\hat{y})\right\} - 1}{\exp[2\pi(\gamma_i+\gamma_s)\hat{\sigma}_{\mathrm{rel}}]^2 - 1}. \tag{24}$$

The ASF can thus still be written as the sum of a shifted δ function (specularly reflected beam) and an associated scattering function $S(\alpha,\beta-\beta_o)$:

$$\begin{aligned}\mathrm{ASF}(\alpha_s,\beta_s;\gamma_i,\gamma_s) &= [A(\gamma_i,\gamma_s)\delta(\alpha,\beta-\beta_o)\\ &\quad + S(\alpha,\beta;\gamma_i,\gamma_s)]|_{\alpha=\alpha_s,\beta=\beta_s},\end{aligned} \tag{25}$$

where

$$S(\alpha,\beta;\gamma_i,\gamma_s) = B(\gamma_i,\gamma_s)\mathcal{F}\{G(\hat{x},\hat{y};\gamma_i,\gamma_s)\exp(-i2\pi\beta_o\hat{y})\}. \tag{26}$$

When numerical solutions of Eq. (26) are required, the parameters γ_s and γ_i have to be specified before performing the Fourier transform. Calculating the scattering distribution over the entire observation space for a given angle of incidence will therefore require a different STF and Fourier transform calculation for every scattering angle.

4 System MTF in the Presence of Surface Scatter

The linear systems formulation of surface scatter phenomena discussed in Sec. 3 not only provides insight and understanding concerning a topic often perceived as being nonintuitive and complicated but also suggests that the image degradation due to the combined effects of diffraction, aberrations, and scattered light can be obtained by merely multiplying the STF by the classical MTF characterizing the image degradation due to diffraction and aberrations. However, there has been legitimate skepticism concerning the accuracy of this simple solution.[44] A few comments are thus in order to justify this simple cascading of transfer functions.

From linear systems theory, we learned that that the transfer functions characterizing various subsystems (or physical processes) can merely be multiplied to obtain the system transfer function if and only if the subsystems (or individual physical processes) are independent and uncorrelated. From the convolution theorem of Fourier transform theory, multiplying transfer functions is equivalent to convolving impulse responses (PSFs in optical imaging applications).

Boreman discusses several MTF contributors in addition to diffraction and aberrations: detector MTF, motion MTF, vibration MTF, turbulence MTF, aerosol MTF, etc.[2] He then discussed cascading (multiplying) MTFs in considerable detail, giving examples where cascading MTFs will provide accurate results as well as examples where cascading MTFs give completely inaccurate results.

It always comes back to whether the various errors (or image degradation mechanisms) are independent and uncorrelated. An additional example is the image degradation due to residual design errors and alignment errors in a telescope. Can we merely convolve the degraded PSF due to the residual design errors with the degraded PSF due to the misalignment errors? Definitely not if the error in both cases is coma. Because they are not uncorrelated. The coma due to residual design errors can actually balance, or partially cancel, the coma due to alignment errors.

Our experience with regard to image degradation due to diffraction, geometrical aberrations, and surface scatter due to residual optical fabrication errors has been "yes" the aerial image of a point source in the focal plane of the telescope is accurately given by the aperture diffraction PSF convolved by the geometrical PSF convolved by the surface scatter PSF.[45] However, since the phase variations induced upon the reflected wavefront by surface roughness are very similar in nature to classical wavefront aberrations, one needs to apply some caution regarding where one draws the line on the surface PSD function between the low spatial frequency figure errors that produce classical aberrations and the high spatial frequency surface roughness that produces scattered light. It is rather arbitrary, but probably safe, to consider this dividing line such that wavefront errors lower than the 22nd, or the 36th, Zernike polynomial is included in the low spatial frequency figure errors (deterministic) and to include the higher Zernike terms with the (statistical) mid or high spatial frequency surface roughness that produces scattered light.

Finally, in a recent publication by Choi and Harvey,[46] it has been shown that, for multielement imaging systems degraded by both surface scatter and aberrations, the composite PSF is obtained in explicit analytic form in terms of convolutions of the geometrical PSF and scaled BRDFs of the individual surfaces of the imaging system. The approximations and assumptions in this formulation are discussed, and the result is compared to the irradiance distribution obtained using commercial software for the case of a two-mirror telescope operating at EUV wavelength. The two results are virtually identical.

We thus proceed by stating with some confidence that the product of the STF with the classical MTF of an imaging system will comprise the system MTF in the presence of surface scatter. Assuming an imaging system with a circular aperture ($D = 50$ mm, $f = 200$ mm) operating at $\lambda = 0.5$ μm, the diffraction-limited MTF is given by:[47]

$$\text{MTF} = \frac{(D^2/2)\{\cos^{-1}(r/D) - (r/D)[1-(r/D)^2]^{1/2}\}}{\pi D^2/4}, \tag{27}$$

and has a cut-off spatial frequency $\xi_c = D/\lambda f = 500$ mm^{-1} as shown in Fig. 4.

Assume also that there is a single reflecting surface with a Gaussian ACV function that produces a TIS = 0.2 (corresponds to an rms roughness of $\sigma = 188$ Å)

$$\text{ACV}_{2D}(\hat{r}) = C_s(\hat{x},\hat{y}) = \sigma^2\text{Gauss}\left\{\frac{\hat{r}}{\hat{\ell}}\right\} = \sigma^2\exp\left[-\pi\left(\frac{\hat{r}}{\hat{\ell}}\right)^2\right], \tag{28}$$

$\ell = 2.0$ mm.

For smooth surfaces, the STF is given by

$$\text{STF} = A + \text{BG}(\hat{x},\hat{y}) \approx A + BC_s(\hat{x},\hat{y})/\sigma^2 \tag{29}$$

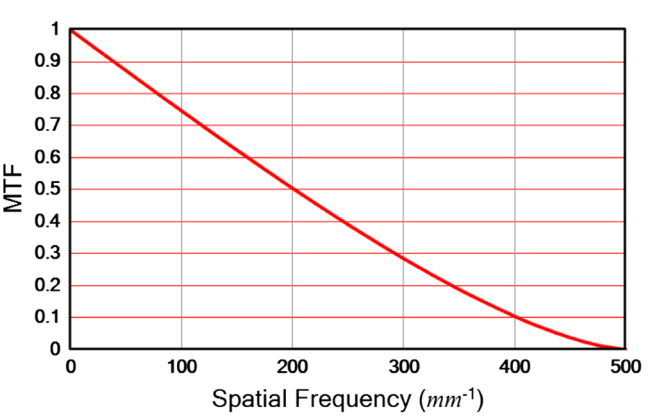

Fig. 4 Diffraction-limited modulation transfer function (MTF) of imaging system with a circular aperture.

$$\mathrm{STF} \approx 0.8 + 0.2\mathrm{Gauss}\left\{\frac{\hat{r}}{\hat{\ell}}\right\}\Bigg|_{r=\rho\lambda f}$$
$$= 0.8 + 0.2\ \exp\left\{-\pi\left(\frac{\rho}{\ell/\lambda f}\right)^2\right\} \quad (30)$$

and illustrated graphically in Fig. 5. We have increased the surface correlation width substantially beyond what it would typically be to enable seeing the nature of the STF at small spatial frequencies.

The system transfer function is given by the product of the classical MTF and the STF

$$H(\hat{x},\hat{y})_{\mathrm{sys}} = \mathrm{MTF} \times \mathrm{STF}. \quad (31)$$

As illustrated in Fig. 6, the system transfer function, as degraded by wide-angle scatter from high spatial frequency microroughness, drops very quickly (at a spatial frequency of about $\ell/\lambda f$) to a value of 1-TIS, then continues diminished proportionately from the classical MTF by that amount

$$H(\hat{x},\hat{y})_{\mathrm{sys}} = (1 - \mathrm{TIS})\mathrm{MTF} \quad \text{for } \xi > \ell/\lambda f. \quad (32)$$

The classical definition of TIS is that fraction of the total reflected radiant power that is scattered out of the specularly reflected beam. Following Davies[48] and Bennett and Porteus,[49] the TIS due to surface scatter from a single moderately rough surface is given by the following analytical expression

$$\mathrm{TIS} = 1 - \exp[-(4\pi\ \cos\ \theta_i\sigma_{\mathrm{rel}}/\lambda)^2]. \quad (33)$$

The above definition of TIS and its paraxial smooth surface approximation

$$\mathrm{TIS} \approx (4\pi\sigma_{\mathrm{rel}}/\lambda)^2 \quad (34)$$

has been discussed extensively in the literature, most recently in Ref. 34. We want to emphasize that the approximate expression in Eq. (34) can only be used for very smooth surfaces. Figure 7 illustrates that the error in Eq. (34) increases exponentially if the rms roughness of the surface exceeds a value of approximately $\sigma_{\mathrm{rel}} = 0.03\lambda$.

Note also that the above expressions for TIS involve the band-limited relative roughness mentioned earlier in Secs. 3.2 and 3.3. This relative roughness and how to calculate it from metrology data are also discussed in detail in Ref. 34.

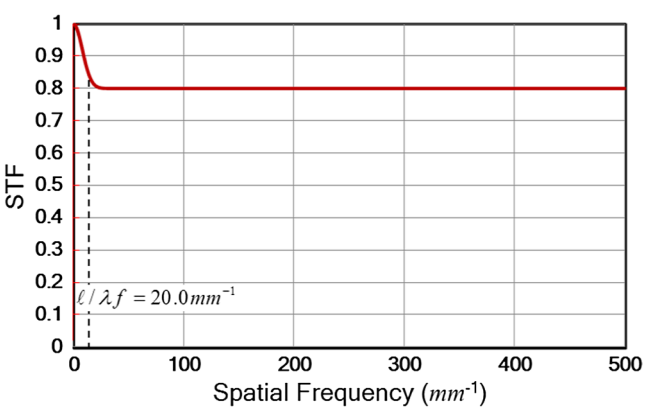

Fig. 5 STF for above example.

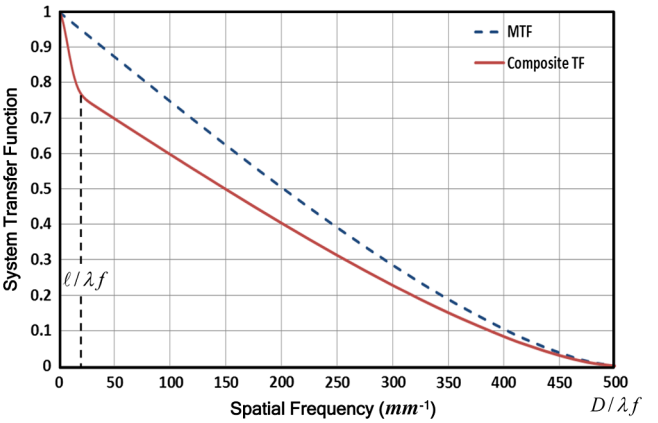

Fig. 6 Illustration of the effect of surface scatter upon the MTF of an imaging system.

5 Parametric Analysis of MTF Behavior for Gaussian Surface PSDs

Since approximations and assumptions were made in the above analysis, we will now provide a parametric analysis of the effect of scatter upon the MTF for surfaces with Gaussian surface PSDs. This parametric analysis will provide insight concerning when one can use the smooth-surface approximation of the OHS surface scatter theory and when one must progress to the MHS or the GHS theory.

5.1 *Variations in Surface Roughness (and TIS)*

Keeping the same optical design parameters ($D = 50$ mm, $f = 200$ mm), and a Gaussian surface ACV function, we will now calculate, and illustrate graphically, variations in STF behavior as we increase the surface roughness (and therefore the amount of light scattered). We have increased the surface ACV length, $\ell = 8.0$ mm, to enable us to more easily see the differences on our parametric plots.

Figure 8 illustrates the STF predicted by the OHS theory Eqs. (1–5) and the smooth-surface approximation to the OHS theory in which $G(\hat{x},\hat{y}) = C_s(\hat{x},\hat{y})/\sigma_s^2$ for increasing

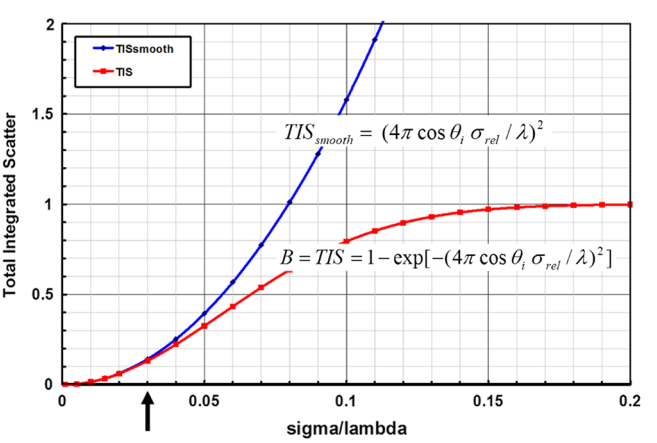

Fig. 7 Illustration of the growth of total integrated scatter (TIS) with increasing surface roughness for normal incidence. Note the exponentially increasing error in Eq. (34) when $\sigma_{\mathrm{rel}} > 0.02\lambda$.

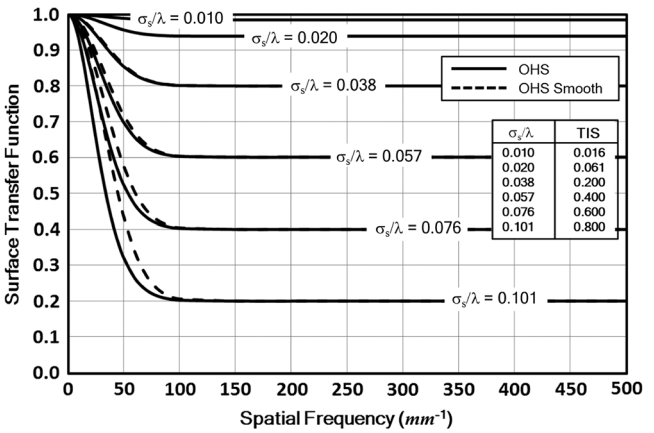

Fig. 8 Variations in STF behavior with increasing surface roughness.

values of surface roughness that results in values of TIS ranging from 0.016 to 0.80. Note that for normal incidence and a Gaussian surface PSD, the smooth-surface approximation to the OHS expression for the STF does not introduce a significant error until TIS > 0.2 and then only for spatial frequencies $\xi < \ell/\lambda f$.

Common image quality criteria might be to specify the maximum allowable degradation due to scatter in the value of the MTF at a specific spatial frequency or to specify the maximum allowable decrease in spatial frequency (due to scatter) at which a specified modulation is maintained. Figure 9 illustrates the composite MTF due to both scatter and diffraction indicating that for a TIS $= 0.2$, there is an 18% decrease in the modulation at a spatial frequency equal to one-half the cut-off spatial frequency and a 24% decrease in the spatial frequency at which a modulation of 0.5 is maintained.

5.2 *Variations in Surface ACV Width*

We have observed a 20% drop in the MTF caused by surface roughness ($\sigma = 188$ Å) sufficient to produce TIS $= 0.2$. The rate at which the MTF drops is determined by the width of the Gaussian surface ACV function. Figure 10 illustrates this variation in MTF behavior with surface ACV width. Note that l does not significantly affect the MTF except at the very short spatial frequencies.

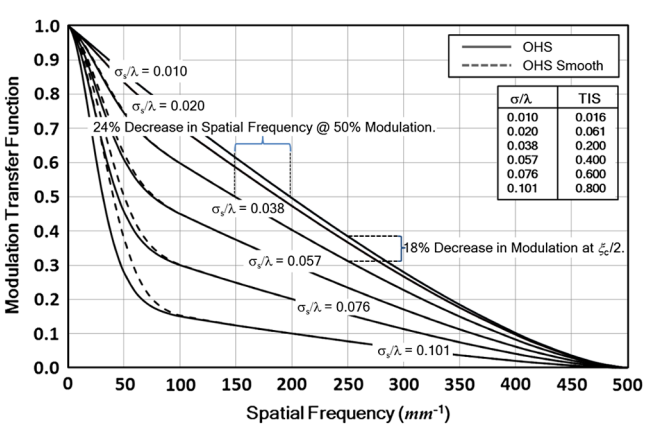

Fig. 9 Variations in MTF behavior with increasing surface roughness.

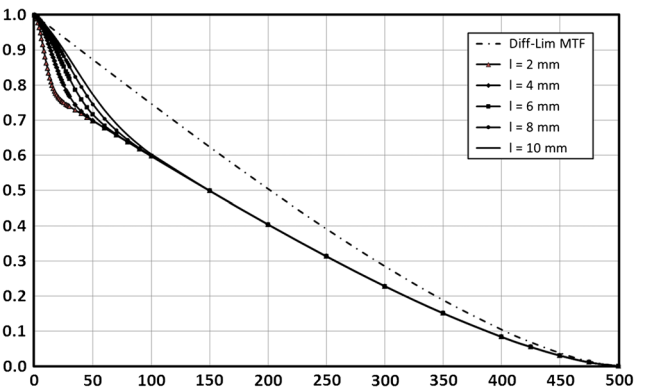

Fig. 10 Variations in MTF behavior with increasing surface correlation width.

5.3 *Variations in Incident Angle*

The modified Harvey–Shack (MHS) surface scatter theory includes the effect of incident angle upon the STF. Figure 11 graphically illustrates the difference in the STF predicted by the OHS theory in which the single STF expressed by Eq. (2) characterizes the scattering process, and the MHS theory which requires a separate STF for each incident angle as expressed in Eq. (10). Parametric plots are presented for several increasingly large incident angles.

Again we have used the same optical design parameters ($D = 50$ mm, $f = 200$ mm), and a Gaussian surface ACV function with $\ell = 2.0$ mm and $\sigma = 188$ Å which produces TIS $= 0.2$ at normal incidence. Figure 11 shows the STF curves where the angle of incidence upon the scattering surface varies from 0 to 20, 30, 40, 50, and 60 deg. Note that the STF predicted by the OHS and the MHS theories are identical at normal incidence. However, as the angle of incidence increases from 0 to 60 deg, the STF increases from 0.8 to almost 0.95. This is a substantial reduction in image degradation. This becomes intuitive when we note that the TIS is reduced from 20% to almost 5% as the angle of incidence is increased. Figure 12 illustrates the corresponding system MTF behavior with increasing incident angle.

In addition to providing insight into the effect of surface scatter upon the MTF, the above parametric curves also assure us that if one is using the simple OHS theory, a worst-case prediction will be obtained.

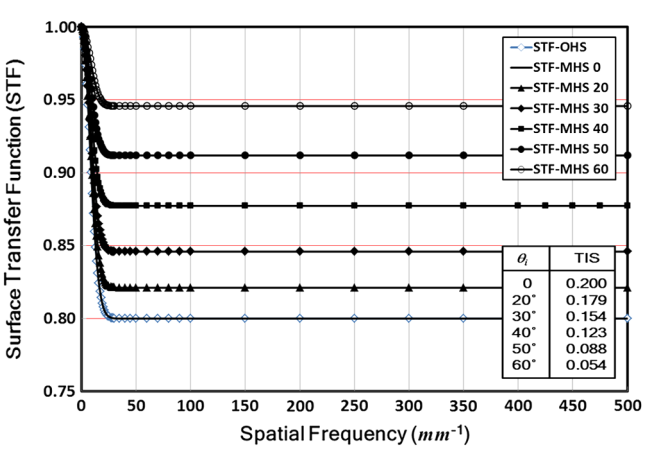

Fig. 11 Variations in STF behavior with increasing incident angle.

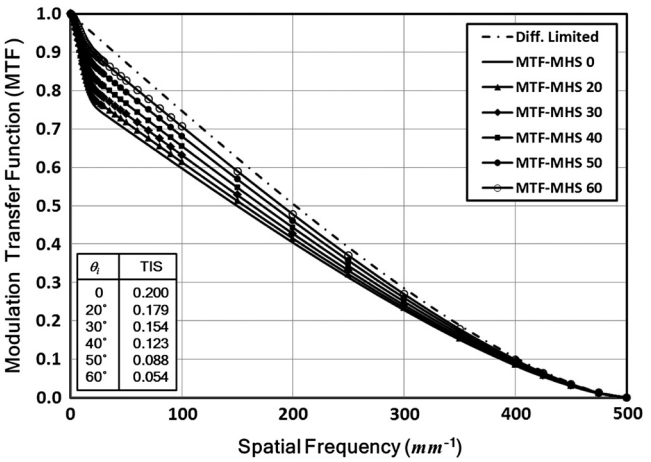

Fig. 12 Variations in composite MTF behavior with increasing incident angle.

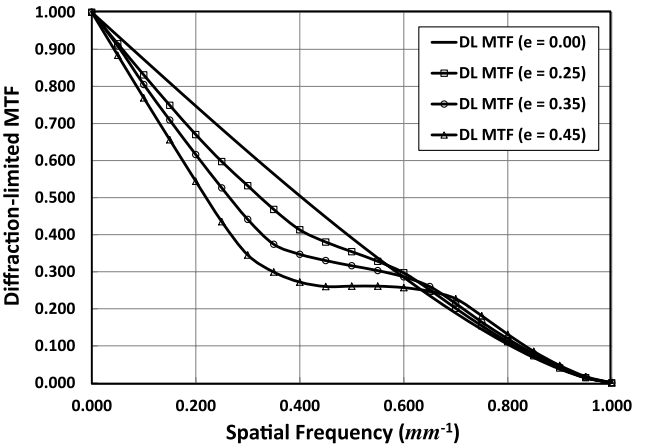

Fig. 13 Effect of the central obscuration upon the diffraction-limited MTF of an annular aperture.

6 Applications Providing Insight into the MTF Behavior Degraded by Surface Scatter

At visible and infrared wavelengths, image degradation due to light scattered from conventionally polished optical surfaces is minimal. However, as the operating wavelength decreases, diffraction effects diminish and image degradation due to surface scatter from residual optical fabrication errors increases dramatically. Also, even at visible wavelengths, significant degradation of the MTF can occur for multielement systems fabricated by unconventional optical fabrication processes, such as diamond-turned metal surfaces. We will thus calculate and illustrate the results for three specific applications: (i) a visible Newtonian telescope with moderately good optical surfaces, (ii) the same Newtonian telescope with state-of-the-art optical surfaces operating at EUV wavelengths, and (iii) a visible ($\lambda = 0.6$ μm) system made up of three diamond-turned off-axis aspheric mirrors where we use the predicted MTF to estimate whether post-polishing will be required to meet a specific image quality requirement.

6.1 *Surface Scatter Effects upon the MTF of a Visible Newtonian Telescope*

Figure 13 shows the effect of a central obscuration upon the normalized diffraction-limited MTF of a two-mirror telescope.[47] Note that there is a substantial decrease in the modulation at the mid spatial frequencies and a slight increase in the modulation at the high spatial frequencies for annual apertures, with these effects being more pronounced for higher obscuration ratios.

Let the telescope diameter, D, focal length, f, and obscuration ratio, ε, of the telescope be given by

$$D = 50 \text{ mm}, \quad f = 500 \text{ mm} \quad \text{and} \quad \varepsilon = 0.25. \tag{35}$$

The cut-off spatial frequency in the MTF of an annular aperture is given by $\xi_c = D/\lambda f$. Figure 14 illustrates the diffraction-limited MTF of our Newtonian telescope with an obscuration ratio of 0.25 for wavelengths of 7000, 6000, 5000, and 4000 Å in the visible spectrum. Since the Newtonian telescope provides a perfect geometrical image on-axis, we have no image degradation due to aberrations.

We will assume that the primary mirror has a Gaussian surface ACV function with an rms roughness, σ_s, and a correlation width, ℓ, given by

$$\sigma_s = 30 \text{ Å}, \qquad l = 1.0 \text{ mm} \tag{36}$$

and ignore any scattering due to the small plane folding secondary mirror.

Even this rather relaxed rms roughness specification of 30 Å on the surface of the primary mirror results in a value of >0.99 for the constant plateau of the STF for all wavelengths >4000 Å as illustrated in Fig. 15. The value of the TIS is also tabulated in Fig. 15 for four wavelengths spanning the visible spectrum.

Multiplying the diffraction-limited MTF illustrated in Fig. 14 by the STF shown in Fig. 15 shows that the degradation of the composite MTF due to surface scatter is barely perceptible even for the shortest visible wavelength as shown in Fig. 16.

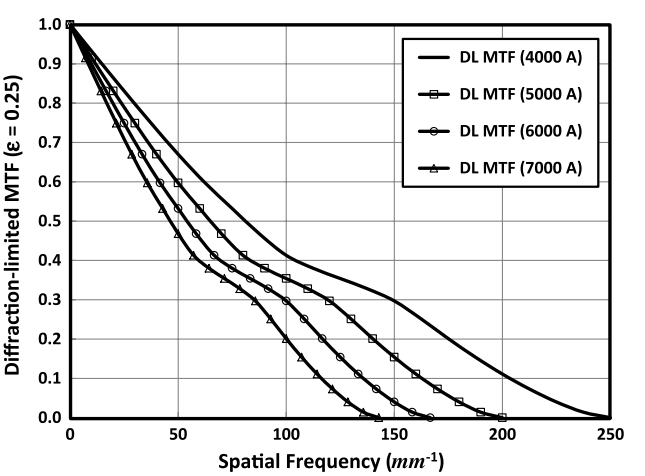

Fig. 14 Effect of wavelength upon the cut-off spatial frequency of the diffraction-limited MTF.

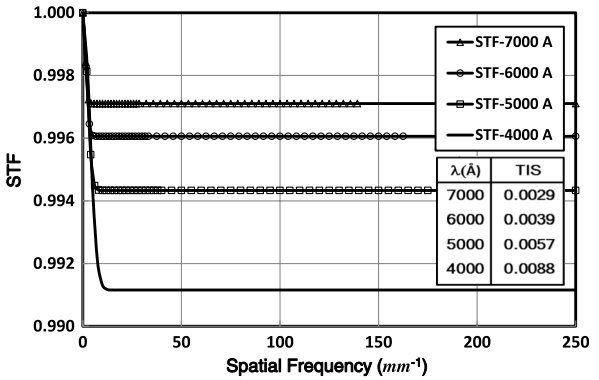

Fig. 15 Illustration of the STF at four visible wavelengths. The corresponding TIS values are also tabulated for the four wavelengths.

6.2 *Surface Scatter Effects upon the MTF of an EUV Newtonian Telescope*

At EUV wavelengths, surface scatter effects can dominate both diffraction effects and geometrical aberrations. The NOAA Solar Ultra Violet Imager (SUVI) program for studying space weather effects due to geomagnetic storms on the surface of the sun is an example where surface scatter effects are of prime importance.[50,51]

Using the same Newtonian telescope as in the previous example, Fig. 17 illustrates the diffraction-limited MTF for wavelengths of 300, 250, 200, 170, 130, and 100 Å in the EUV spectrum. Note the extremely large cut-off spatial frequencies which scale inversely with the wavelength. Since the Newtonian telescope provides a perfect geometrical image on-axis, we are still ignoring image degradation due to aberrations.

Tightening the rms roughness specification to 8 Å and maintaining the 1.0-mm correlation length on the primary mirror of the Newtonian telescope results in a STF at the six different EUV wavelengths as shown in Fig. 18. Note that the TIS varies from just over 10% at the longest wavelength of 300 Å to almost 64% at the shortest wavelength of 100 Å. We are again ignoring any scattering due to the small plane folding secondary mirror.

Finally, we obtain the composite MTF of the EUV Newtonian telescope by multiplying the MTFs and the

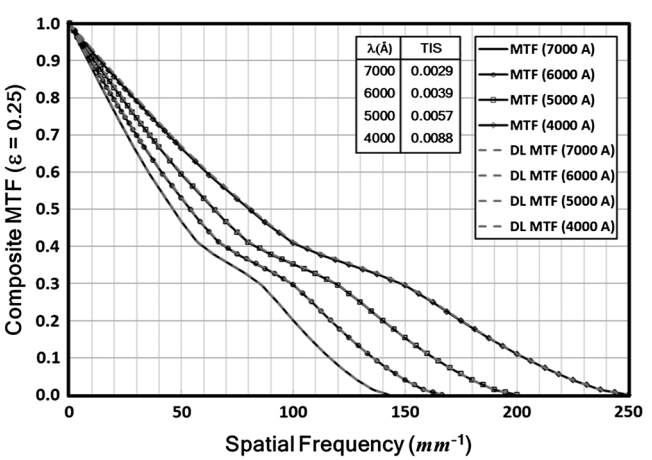

Fig. 16 Illustration of the negligible effect of surface scatter upon the MTF at visible wavelengths.

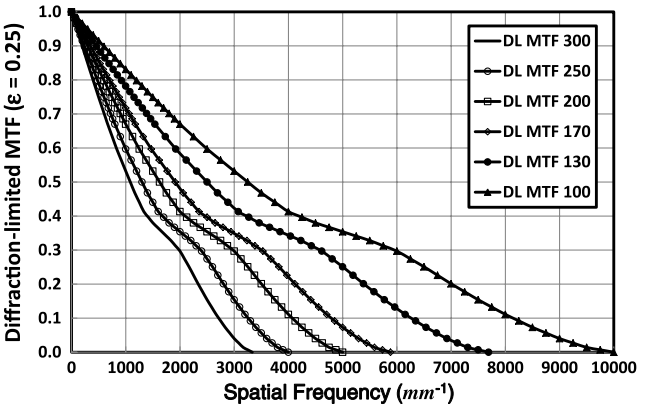

Fig. 17 Effect of wavelength upon the cut-off spatial frequency of the diffraction-limited MTF.

STFs shown in Figs. 17 and 18. A slight reduction of the 8 Å rms roughness to 7.85 Å ensures that the modulation at a spatial frequency of 2000 mm^{-1} will be at least 0.25 for all wavelengths between 300 and 100 Å. These composite MTFs are shown in Fig. 19.

Plotting the modulation versus wavelength at a spatial frequency of 2000 mm^{-1}, as shown in Fig. 20, provides insight concerning the relative importance of diffraction and scattering over the EUV spectral range of interest. Note in Fig. 20 that at a spatial frequency of 2000 mm^{-1} surface scatter limits the modulation at the low end of the EUV spectrum and diffraction limits the modulation at the high end of the EUV spectrum, with the intermediate wavelengths exhibiting the highest modulation.

6.3 *Surface Scatter Effects upon the MTF for a Three-Element Diamond-Turned System*

Suppose we need to establish optical fabrication tolerances for four reflective mirrors making up a 4× a focal, unobscured subsystem which will meet the following MTF requirements at a wavelength of 6000 Å:

$$\text{Modulation} > 0.60 \quad \text{at} \quad 40.0 \text{ cycles/mrad}. \tag{37}$$

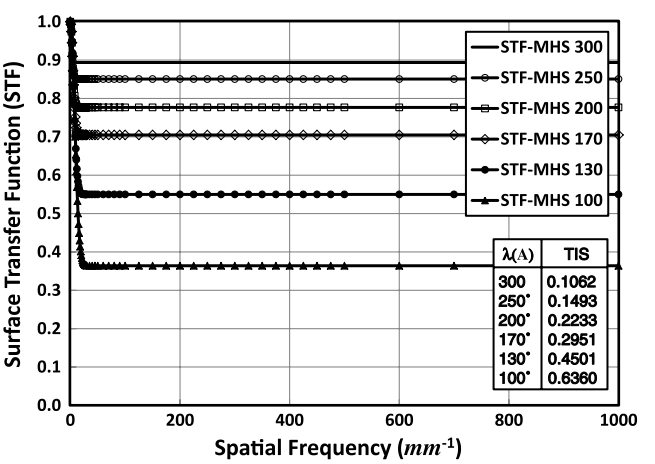

Fig. 18 Illustration of STF caused by an 8-Å rms surface roughness on the primary mirror. Note that almost 64% of the extreme ultraviolet (EUV) radiation is scattered out of the image core for the shortest wavelength.

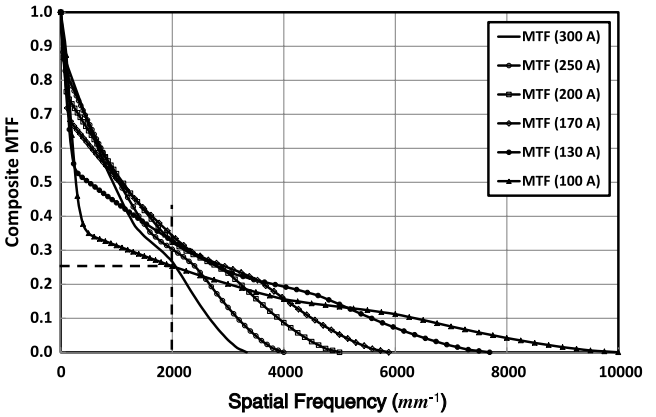

Fig. 19 Illustration of the composite MTF of a Newtonian telescope caused by surface scatter and diffraction for six different wavelengths in the EUV spectrum ($\epsilon = 0.25$ and $\sigma = 7.85$ Å).

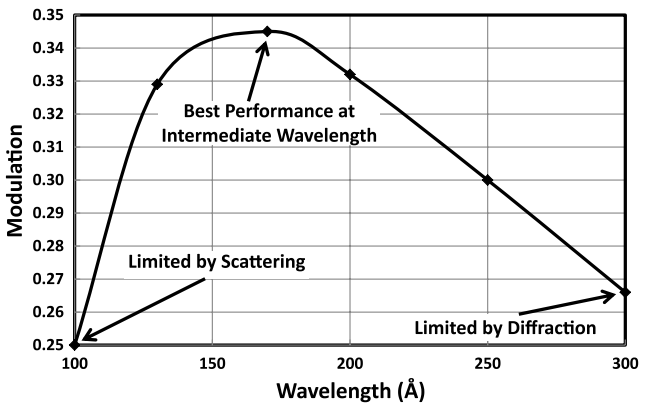

Fig. 20 At a spatial frequency of 2000 mm^{-1}, surface scatter limits the value of the MTF at the short wavelengths, diffraction limits the value at long wavelengths, and the highest performance is achieved in the middle of the EUV spectrum.

The first element of the subsystem is a folding flat (object-plane scanning element) that will be left out of the following analysis for convenience. This is justified based upon the negligible degradation to the MTF due to surface scatter of state-of-the art mirrors at visible wavelengths shown in the Sec. 6.1. The entrance pupil lies in front of an off-axis paraboloidal primary mirror. An off-axis hyperboloidal secondary mirror then produces an internal focus. The light is then collected and collimated by an off-axis paraboloidal tertiary mirror. All three of these mirrors are off-axis segments of conic surfaces of revolution with a common axis of rotation. The entrance pupil has a diameter of 86.0 mm,

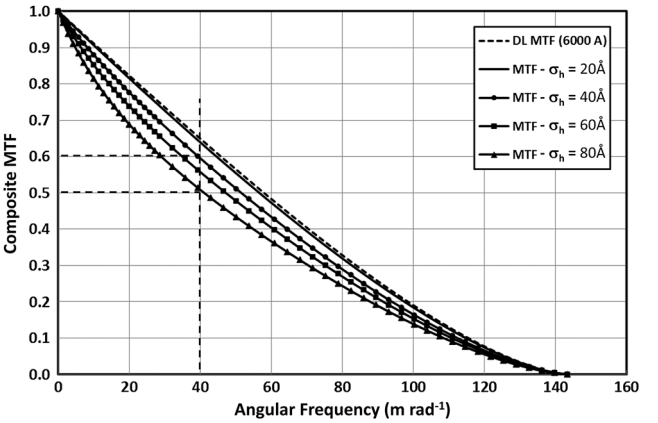

Fig. 21 Illustration of the sensitivity of the MTF of a three-element system of diamond-turned aspheres to the residual rms microroughness ($\lambda = 6000$ Å).

and the exit pupil has a diameter of 21.5 mm, giving the afocal system a magnification of 1/4.

Noll and Glenn[52] have shown that optically polished glass samples exhibit two scales of roughness and that each scale can reasonably be characterized by an exponential ACV function

$$\mathrm{ACV} = \sigma_h^2 \exp(-r/\ell_h) + \sigma_m^2 \exp(-r/\ell_m), \tag{38}$$

where $r = \sqrt{x^2 + y^2}$ is the radial shift parameter, σ_h is the high spatial frequency rms microroughness, ℓ_h is the high spatial frequency autocovariance length, σ_m is the midspatial frequency rms roughness and ℓ_m is the mid spatial frequency autocovariance length.

Excellent agreement with experimental results has previously been obtained using this model for several different applications.[53–57]

Our approach is now to proceed to perform parametric performance predictions as a function of the four surface parameters indicated in the above equation for the surface ACV function. Following the approach outlined in Sec. 4 for a single mirror, we will simplify things by assuming that all three mirrors have the same ACV function and will merely multiply the three individual mirror STFs to approximate the three-element STF. This will allow us to estimate the optical fabrication tolerances necessary to satisfy the image quality requirement.

As an example, the MTF will first be calculated for four separate cases where only the high spatial frequency microroughness is varied. The other three surface parameters will be held constant, i.e.,

$$\begin{aligned}
&\text{Case1:}\quad \sigma_m = 200 \quad,\quad \ell_m = 1.00 \text{ mm} \qquad \text{Case2:}\quad \sigma_m = 200 \quad,\quad \ell_m = 1.00 \text{ mm}\\
&\qquad\quad \sigma_h = 20 \quad,\quad \ell_h = 0.01 \text{ mm} \qquad\qquad\quad \sigma_h = 40 \quad,\quad \ell_h = 0.01 \text{ mm}\\
&\qquad\quad \text{For all three (3) mirrors} \qquad\qquad\quad \text{For all three (3) mirrors}\\
&\text{Case3:}\quad \sigma_m = 200 \quad,\quad \ell_m = 1.00 \text{ mm} \qquad \text{Case4:}\quad \sigma_m = 200 \quad,\quad \ell_m = 1.00 \text{ mm}.\\
&\qquad\quad \sigma_h = 60 \quad,\quad \ell_h = 0.01 \text{ mm} \qquad\qquad\quad \sigma_h = 80 \quad,\quad \ell_h = 0.01 \text{ mm}\\
&\qquad\quad \text{For all three (3) mirrors} \qquad\qquad\quad \text{For all three (3) mirrors}
\end{aligned} \tag{39}$$

Figure 21 indicates that in order to meet the requirement expressed in Eq. (37), the diamond-turned surfaces would have to be post-polished to a microroughness of $\sigma_h \leq 40$ Å; however, if the requirement could be reduced to a modulation $\geq$0.50 at 40.0 cycles/mrad, then post-polishing would not be required provided the diamond-turned surfaces had an

rms microroughness of $\sigma_h \leq 80$ Å;. Since post-polishing is a labor-intensive and time-consuming process, this would save considerable cost and schedule for the program. Similar sensitivity analyses could be done for the other three optical surface parameters.

7 Effect of (Nonsurface) Scatter upon the Optical System MTF

Thus far in this article, we have been using surface scatter theory to predict the STF from optical surface metrology data. For particulate scatter effects due to contaminated or dirty optical surfaces, a theoretical, or empirical, approach to characterizing the scatter behavior and predicting the bidirectional scatter distribution function (BSDF) can be employed. However, there are a multitude of painted, coated, processed, or natural surfaces and materials used as structural elements or baffles in optical systems that produce stray light by various (unknown) subsurface or bulk scattering mechanisms. There is also stray light or scattering effects from background elements in the scene being imaged for a given application.

For such materials, one must have at least limited measured BSDF data, or an empirical BSDF model in order to predict the optical performance of an imaging system. With these BSDF data or models provided as input, there are extensive optical analysis software packages such as FRED, ASAP, or TracePro[37–39] that are capable of predicting the irradiance distribution in the focal plane of very complex optical systems imaging very complex scenes, under virtually arbitrary illumination conditions. If the MTF is desired as the image quality criterion for a complex system with stray light sources other than surface scatter from well characterized surfaces, the following procedure would be required.

Point source illumination can be used to predict the irradiance distribution in the focal plane. This PSF can then be Fourier transformed to obtain the OTF as illustrated schematically in Fig. 1. The modulus of this OTF is the desired MTF.

8 Summary

We first reviewed the historical background of surface scatter theory and then discussed the evolution of a linear systems formulation of surface scatter theory that characterizes the surface scatter process with a STF. The classical MTF of an imaging system can merely be multiplied by this STF to obtain the composite MTF as degraded by diffraction, geometrical aberrations, and surface scatter effects. We then presented a parametric analysis of the effect of scattered light upon the MTF as the rms surface roughness, surface correlation length, and the incident angle was varied. The resulting parametric plots provided insight and understanding not readily available in the existing literature. We then modeled the degradation of the MTF due to surface scatter from residual optical fabrication errors for three specific examples: (1) the MTF of a Newtonian telescope was shown to be negligibly degraded when illuminated by visible light if the rms surface roughness of the primary mirror is <30 Å; (2) the MTF of a Newtonian telescope with a state-of-the-art primary mirror ($\sigma_s < 8$ Å) was then modeled at six EUV wavelengths and shown to be severely degraded by surface scatter (TIS > 0.6) at the shorter wavelengths while diffraction dominated scatter effects at the larger EUV wavelengths; (3) finally, a three-element system of diamond-turned off-axis aspheres illuminated by visible light at a wavelength of 600 nm was evaluated and the predicted MTF was used to determine whether post-polishing would be required to meet a specific image quality requirement.

9 Conclusions

Scattered light from residual optical fabrication errors does indeed degrade the MTF of imaging systems and is easily calculated from surface metrology data such as the surface ACV function. However, the effect is negligible for moderately good optical surfaces operating at visible wavelengths. The ratio of rms surface roughness to wavelength, σ/λ, is the main driver in the effect of scattered light upon the MTF of an imaging system; hence, surface scatter effects can dominate both the diffraction effects and the geometrical aberrations in the degradation of short wavelength EUV imaging systems. Particularly valuable in many practical optical engineering applications is using the degradation of the MTF due to scattered light to determine whether post-polishing of diamond-turned optics is necessary in order to satisfy specific image quality requirements. There is a huge program savings, in terms of both cost and schedule, for many advanced optical systems if post-polishing can be shown to be unnecessary.

Acknowledgments

I would like to thank Photon Engineering, LLC, for funding this study, and Richard Pfisterer in particular for his encouragement and many stimulating discussions on the topic of the effects of stray light upon the MTF of imaging systems.

References

1. C. S. Williams and O. A. Becklund, *Introduction to the Optical Transfer Function*, SPIE Press, Bellingham, WA (2002).
2. G. D. Boreman, *Modulation Transfer Function in Optical, and Electro-optical Systems*, Vol. TT52, SPIE Press, Tutorial Texts in Optical Engineering, Bellingham, WA (2001).
3. V. N. Mahajan, *Optical Imaging and Aberrations Part II: Wave diffraction Optics*, SPIE Press, Bellingham, WA (2001).
4. E. Salvagnini et al., "Quantification of scattered radiation in projection mammography: four practical methods compared," *Med. Phys.* **39**(6), 3167–3180 (2012).
5. K. Kamiya et al., "Clinical evaluation of optical quality and intraocular scattering after posterior chamber phakic intraocular lens implantation," *Invest. Ophthalmol. Vis. Sci.* **53**(6), 3161–3166 (2012).
6. S. O. Rice, "Reflection of electromagnetic waves from slightly rough surfaces," *Commun. Pure Appl. Math.* **4**(2–3), 351–378 (1951).
7. E. L. Church, H. A. Jenkinson, and J. M. Zavada, "Relationship between surface scattering and microtopographic features," *Opt. Eng.* **18**(2), 125–136 (1979).
8. J. C. Stover, *Optical Scattering, Measurement and Analysis*, 3rd ed., SPIE Optical Engineering Press, Bellingham, WA (2012).
9. P. Beckmann and A. Spizzichino, *The Scattering of Electromagnetic Waves from Rough Surfaces*, Pergamon Press, New York (1963).
10. J. E. Harvey, "Light-scattering characteristics of optical surfaces," Ph.D. Dissertation, University of Arizona (1976).
11. J. E. Harvey, "Surface scatter phenomena: a linear, shift-invariant process," *Proc. SPIE* **1165**, 87–99 (1989).
12. J. E. Harvey, E. C. Moran, and W. P. Zmek, "Transfer function characterization of grazing incidence optical systems," *Appl. Opt.* **27**(2), 1527–1533 (1988).
13. T. M. Elfouhaily and C. A. Guerin, "A critical survey of approximate scattering wave theories from random rough surfaces," *Waves Random Media* **14**(4), R1–R40 (2004).
14. C. L. Vernold and J. E. Harvey, "A modified Beckmann-Kirchhoff scattering theory for nonparaxial angles," *Proc. SPIE* **3426**, 51–56 (1998).
15. J. E. Harvey, A. Krywonos, and C. L. Vernold, "Modified Beckmann-Kirchhoff scattering model for rough surfaces with large incident and scattered angles," *Opt. Eng.* **46**(7), 078002 (2007).
16. H. Ragheb and E. R. Hancock, "Rough surface correction and re-illumination using the modified Beckmann model," in *Proc. 10th*

Int. Conf. Computer Analysis of Images and Patterns, Vol. 2756, pp. 98–106, Groningen, The Netherlands (2003).
17. H. Ragheb and E. R. Hancock, "Rough surface estimation using the Kirchhoff model," in *Image Analysis*, J. Bigun and T. Gustavsson, Eds., SCIA 2003, LNCS, Vol. 2749, pp. 477–484, Springer-Verlag, Berlin, Heidelberg (2003).
18. P. Hermansson, G. Forssell, and J. Fagerstrom, *A Review of Models for Scattering from Rough Surfaces*, Scientific Report FOI-R-0988-SE by the Swedish Defense Research Agency, ISSN 1650-1942, p. 61 (2003).
19. A. Robles-Kelly and E. R. Hancock, "Radiance function estimation for object classification," *Prog. Pattern Recognit. Image Anal. Appl.*, A. Sanfeliu, Ed., CIARP 2004, LNCS, Vol. 3287, pp. 67–75, Springer-Verlag, Berlin, Heidelberg (2004).
20. A. Robles-Kelly and E. R. Hancock, "Estimating the surface radiance function from single images," *Graph. Models* **67**(6), 518–548 (2005).
21. H. Ragheb and E. R. Hancock, "Surface radiance correction for shape from shading," *Pattern Recogn.* **38**(10), 1574–1595 (2005).
22. H. Ragheb and E. R. Hancock, "Adding subsurface attenuation to the Beckmann-Kirchhoff theory," in *Proc. Pattern Recognition, and Image Analysis, Part 2*, J. S. Marques, Ed., IbPRIA 2005. LNCS, Vol. 3523, pp. 247–254, Springer-Verlag, Berlin, Heidelberg (2005).
23. H. Ragheb and E. R. Hancock, "Testing new variants of the Beckmann-Kirchhoff model against radiance data," *Comput. Vision Image Underst.* **102**(2), 145–168 (2006).
24. H. Ragheb and E. Hancock, "The modified Beckmann-Kirchhoff scattering theory for rough surface analysis," *Pattern Recogn.* **40**(7), 2004–2020 (2007).
25. J. E. Harvey et al., "Diffracted radiance: a fundamental quantity in a non-paraxial scalar diffraction theory," *Appl. Opt.* **38**(31), 6469–6481 (1999).
26. J. E. Harvey et al., "Diffracted radiance: a fundamental quantity in a non-paraxial scalar diffraction theory: errata," *Appl. Opt.* **39**(34), 6374–6375 (2000).
27. A. Krywonos, "Predicting surface scatter using a linear systems formulation of non-paraxial scalar diffraction," Ph.D. Dissertation, p. 224, University of Central Florida (2006).
28. A. Krywonos, J. E. Harvey, and N. Choi, "Linear systems formulation of surface scatter theory for rough surfaces with arbitrary incident and scattering angles," *J. Opt. Soc. Am. A* **28**(6) 1121–1138 (2011).
29. J. W. Goodman, *Introduction to Fourier Optics*, 2nd ed., McGraw-Hill, New York (1996).
30. J. D. Gaskill, *Linear Systems, Fourier Transforms, and Optics*, Wiley, New York (1978).
31. J. A. Ratcliff, "Some aspects of diffraction theory and their application to the ionosphere," in *Reports of Progress in Physics*, A. C. Strickland, Ed., Vol. XIX, The Physical Society, London (1956).
32. J. E. Harvey and C. L. Vernold, "Description of diffraction grating behavior in direction cosine space," *Appl. Opt.* **37**, 8158–8160 (1998).
33. J. E. Harvey and A. Krywonos, "Radiance: the natural quantity for describing diffraction and propagation," *Proc. SPIE* **6285**, 628503 (2006).
34. J. E. Harvey et al., "Total integrated scatter from surfaces with arbitrary roughness, correlation widths, and incident angles," *Opt. Eng.* **51**(1), 013402 (2012).
35. F. E. Nicodemus, "Reflectance nomenclature and directional reflectance and emissivity," *Appl. Opt.* **9**(6), 1474–1475 (1970).
36. *Users Manual for APART/PADE*, Version 8.6, pp. 5–2, Breault Research Organization, Tucson, AZ (1987).
37. *ASAP Reference Manual*, p. 3–43, Breault Research Organization, Tucson, AZ (1990).
38. *FRED User's Manual*, Version 9.110, Photon Engineering LLC, Tucson, AZ (2010).
39. *TracePro User's Manual*, Release 3.0, p. 7.12, Lambda Research Corporation, Littleton, MA (1998).
40. *ZEMAX User's Guide*, August 2007, p. 391, ZEMAX Development Corp., Bellevue, WA (2007).
41. P. Glenn et al., "Performance prediction of AXAF technology mirror assembly using measured mirror surface errors," *Proc. SPIE* **27**, 1539–1543 (1988).
42. J. E. Harvey and P. L. Thompson, "Generalized Wolter type I design for the solar X-ray imager (SXI)," *Proc. SPIE* **3766**, 173–183 (1999).
43. J. E. Harvey et al., "Scattering from moderately rough interfaces between two arbitrary media," *Proc. SPIE* **7794**, 77940V (2010).
44. J. E. Harvey and A. Krywonos, "A systems engineering analysis of image quality," *Proc. SPIE* **4093**, 379–388 (2000).
45. J. E. Harvey et al., "The solar X-ray imager (SXI) on GOES-13: design, analysis, and on-orbit performance," *Proc. SPIE* **6689**, 668901 (2007).
46. N. Choi and J. E. Harvey, "Image degradation due to surface scatter in the presence of aberrations," *Appl. Opt.* **51**(5), 535–546 (2012).
47. V. N. Mahajan, *Optical Imaging, and Aberrations: Part II Wave Diffraction Optics*, pp. 96, SPIE Press, Bellingham, WA (2001).
48. H. Davies, "The reflection of electromagnetic waves from a rough surface," *Proc. Inst. Elec. Engrs.* **101**(Pt. III), 209–214 (1954).
49. H. E. Bennett and J. O. Porteus, "Relation between surface roughness and specular reflectance at normal incidence," *J. Opt. Soc. Am.* **51**(2), 123–129 (1961).
50. J. E. Harvey et al., "Image degradation due to scattering effects in two-mirror telescopes," *Opt. Eng.* **49**(6), 063202 (2010).
51. D. Martinez-Galarce et al., "A novel forward-model technique for estimating EUV imaging performance: design and analysis of the SUVI telescope," *Proc. SPIE* **7732**, 773237 (2010).
52. R. J. Noll and P. E. Glenn, "Mirror surface autocovariance functions and their associated visible scattering," *Appl. Opt.* **21**(10), 1824–1838 (1982).
53. A. Kotha and J. E. Harvey, "Enhanced EUV performance of Wolter type II telescopes," *Proc. SPIE* **2011**, 34–46 (1993).
54. W. J. Gressler and J. E. Harvey, "Conical foil telescope performance predictions for space astronomy applications," *Proc. SPIE* **2011**, 182–192 (1993).
55. J. E. Harvey, "Scattering effects in x-ray imaging systems," *Proc. SPIE* **2515**, 246–272 (1993).
56. J. E. Harvey, K. L. Lewotsky, and A. Kotha, "Effects of surface scatter on the optical performance of x-ray/EUV synchrotron beamline mirrors," *Appl. Opt.* **34**(16), 3024–3032 (1995).
57. J. E. Harvey, K. L. Lewotsky, and A. Kotha, "Performance predictions of a Schwarzschild imaging microscope for soft x-ray applications," *Opt. Eng.* **35**(8), 2423–2436 (1996).

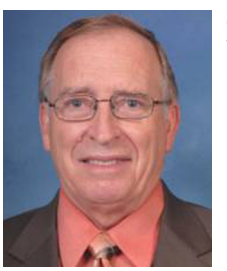

James E. Harvey is a retired associate professor in the College of Optics and Photonics at the University of Central Florida and currently a senior optical engineer with Photon Engineering LLC in Tucson, AZ. He has a PhD in optical sciences from the University of Arizona and is credited with over 200 publications and conference presentations in the areas of diffraction theory, surface scatter phenomena, adaptive optics, wavefront sensing, beam sampling technology, optical properties of materials, phased telescope arrays, and x-ray/EUV imaging systems. He is a member of OSA and a Fellow and past board member of SPIE.